Si@Au Core–Shell Nanostructures: Toward a New Platform for Controlling Optical Properties at the Nanoscale

Wajdi Chaâbani, Julien Proust, Samuel Ouellet, Artur Movsesyan, Jérémie Béal, Renaud Bachelot, Tao Xu, Anne-Laure Baudrion, Pierre-Michel Adam, Denis Boudreau, et al.

▶ To cite this version:

Wajdi Chaâbani, Julien Proust, Samuel Ouellet, Artur Movsesyan, Jérémie Béal, et al.. Si@Au Core–Shell Nanostructures: Toward a New Platform for Controlling Optical Properties at the Nanoscale. Journal of Physical Chemistry C, 2021, 125 (37), pp.20606 - 20616. 10.1021/acs.jpcc.1c06182 . hal-03633250

HAL Id: hal-03633250

https://hal.science/hal-03633250v1

Submitted on 6 Apr 2022

Si@Au Core–Shell Nanostructures: Toward a New Platform for Controlling Optical Properties at the Nanoscale

Wajdi Chaâbani, Julien Proust, Samuel Ouellet, Artur Movsesyan, Jérémie Béal, Renaud Bachelot, Tao Xu, Anne-Laure Baudrion, Pierre-Michel Adam, Denis Boudreau, et al.

To cite this version:

Wajdi Chaâbani, Julien Proust, Samuel Ouellet, Artur Movsesyan, Jérémie Béal, et al.. Si@Au Core–Shell Nanostructures: Toward a New Platform for Controlling Optical Properties at the Nanoscale. Journal of Physical Chemistry C, American Chemical Society, 2021, 125, pp.20606 - 20616. 10.1021/acs.jpcc.1c06182 . hal-03633250

Si@Au Core−Shell Nanostructures: Toward a New Platform for Controlling Optical Properties at the Nanoscale

Wajdi Chaâbani, Julien Proust,* Samuel Ouellet, Artur Movsesyan, Jérémie Béal, Renaud Bachelot, Tao Xu, Anne-Laure Baudrion, Pierre-Michel Adam, Denis Boudreau, Abdallah Chehaidar, and Jérôme Plain*

Cite This: https://doi.org/10.1021/acs.jpcc.1c06182

ABSTRACT: Hybrid dielectric−metal colloid nanoparticle heterostructures have recently attracted attention in both fundamentals and applications. In this paper, we developed a new approach based on mechanical grinding and chemical synthesis in order to obtain hybrid dielectric−metal nanoparticles. By increasing the amounts of the stabilizing agent (polyvinylpyrrolidone (PVP)), three different types of hybrid colloidal structures were obtained, Si/Au core−island, core−shell, and core−shell oligomers heterostructures, respectively. The obtained colloidal heterostructures were analyzed by dynamic light scattering (DLS) and scanning electron microscope (SEM) measurements. Moreover, the optical properties of hybrid nanostructure have been carefully studied. A splitting was observed in the extinction spectra of colloidal solutions for different Si/Au colloidal heterostructures compared to Si colloidal nanoparticles, attributed to the hybridization of plasmon. Thanks to photolithographic and drop-cast deposition techniques on a substrate, we were able to locate the colloidal nanoparticles heterostructures and to measure the backward scattering spectra using single-particle dark-field scattering spectroscopy. To better understand scattering results, FDTD simulations of scattering cross-section and electric near-field distributions were performed. As is well-known, the scattering spectrum of the pristine Si core is dominated by electric and magnetic dipolar modes in the visible region. More importantly, the scattering spectra of Si/Au core−island and core−shell support several phenomena such as collective magnetic dipolar modes and multiple Fano lineshapes. Our finding highlights the potential of our dielectric−metal heterostructures as a platform for studying light−matter interactions at the nanoscale.

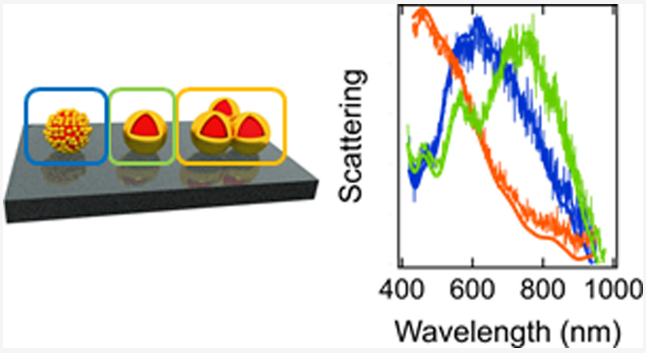

1. INTRODUCTION

Gold, silver, and aluminum nanoparticles (NPs) attracted many attention during the recent decades,[1−3] mainly due to their strong optical response to the electric field of the light, known as localized surface plasmon resonance (LSPR). At optical frequencies, pure metals present a strong absorption leading to heating effects.[4] Absorption-induced heating is a limiting effect for many applications such as exalted fluorescence or chemical analysis. On the other hand, it is an effect that is widely desired in the curative treatment of cancer or the thermo-induced chemistry at the nanoscale. To overcome such limitations and simultaneously exploit similar resonant optical properties, one possible alternative is to use high-refractive-index dielectric nanoparticles. Silicon nanoparticles present strong magnetic and electric Mie-resonant modes in the visible range.[5,6] Tsuchimoto et al.[7] demonstrated that Si/SiO$_2$ core−shell nanoparticles exhibit a Fano resonance associated with ultrahigh scattering directionality. Moreover, silicon nanospheres dimer exhibits directional Fano resonance induced by the coupling between electric and magnetic dipole modes.[8] Furthermore, an all-dielectric nanospheres oligomer exhibits well-pronounced Fano resonances with a strong suppression of the scattering cross-section.[9] When the silicon nanoparticles are almost in contact, the phenomena called magnetically induced transparency (MIT) appears. MIT exhibits a near-zero reflection and near-perfect transmission inducing a light propagation without extra phase change.[10]

Received: July 11, 2021

Sugimoto et al.[11] demonstrated that Si NPs on a metal thin film structure can act as a broadband nanoantenna. Moreover, such a structure can enhance luminescence of an emitter in the gap in a wide spectral range.

Hybrid nanoantennas, which combine high-index NPs with plasmonic elements, demonstrate both electric and magnetic multipolar resonances. Feng et al.[12] demonstrated that an ultrathin electric conductive precoating can dramatically modifying the optical properties of silicon nanosphere. Indeed, a broadening of electric dipole and a reduction of strength of magnetic resonance appears. Also, they found that unidirectional Fano resonant scattering occurs with a 9 nm thin Au coating. Simultaneously, Feng et al.[13] demonstrated that the Au/Si core−shell nanosphere can be used as an ideal magnetic dipole scattering. Recently, Yang et al.[14] theoretically demonstrated the Au/Si core−shell nanostructures present nonlinear optical properties, particularly for second harmonic generation (SHG). Miroshnichenko[15] theoretically studied, in both cases, dielectric−metal and metal−dielectric core−shell spherical heterostructures where the local field enhancement takes place in out-of-resonance regions (”dark states”) and has been attributed to Fano resonance. Sancho-Parramon et al.[16] demonstrated that a single-layered concentric core−shell particle presents an inherent Fano profiles in the scattering spectra. Such a behavior is possible when sphere and cavity modes spectrally overlap. Various methods of synthesis of such hybrid Si/Au core−shell NPs have been proposed.

Recently, an ablation laser in a liquid[17−19] and on a multilayer thin Si/Au films,[20,21] as well as the photochemical synthesis,[22] has been utilized for growing Si/Au core−shell nanoparticles. However, these methods do not fully succeed to produce a complete Au shell on silicon crystalline nanoparticles. The difficulty arises mainly due to some problem in the gold attachment with the silicon surface nanoparticles. To the best of our knowledge, a simple method for producing the Si/Au core−islands, core−shell, and/or core−shell oligomers nanoparticles with large-scale quantities and high colloidal stability and purity in solution has not been reported so far.

In this study, we successful synthesize different Si/Au heterostructures geometries: core−islands, core−shell, and core−shell oligomers. The Si nanoparticles are mechanically fabricated using a blender, as reported in our previous work, with an average diameter 170 nm.[5] We will then focus on the study of the optical properties of various heterostructures through UV−vis extinction and single-particle dark-field spectroscopies.

2. EXPERIMENTAL SECTION

2.1. Chemicals. Ammonium hydroxide (NH_4OH, 28−30 wt %), (3-aminopropyl)triethoxysilane (APTES, 98%), tetrakis(hydroxymethyl), sodium hydroxide (NaOH, > 97%), gold(III) chloride trihydrate ($HAuCl_4 \cdot 3\ H_2O$, >99.9%), potassium carbonate (K_2CO_3, 99.0%), formaldehyde solution (CH_2O, 37%), poly(vinylpyrrolidone) (K10) (average molecular weight of 10 kg/mol), acetic acid (CH_3COOH, 99.7%), and tetrakis(hydroxymethyl)phosphonium chloride solution (THPC) ($(HOCH_2)_4PCl$) were purchased from Sigma-Aldrich and used without further purification. The silicon pellets (99.9999% purity) were purchased from Alfa Aesar. Ultrapure water was purified by a Millipore Milli-Q water system (has a resistivity of 18.2 $M\Omega \cdot cm^{-1}$ at 25 °C) and was used for all experiments.

2.2. Synthesis of Silicon−NH_2. The Si NPs were mixed with APTES to generate an amino group terminated surface. First, 28 mL of Si NPs was heated at 100 °C and stirred for 10 min. The heating step is important for forming more thickness of silica layer (i.e., more oxygen atoms termination on the Si surface) coated the Si core. Then, 8 μL of 1% APTES was added into the suspension of 28 mL of the Si NPs solution with continuous stirring at 25 °C. After 1 h, 1 mL of a NH_4OH solution was added and let to react 24 h to allow the condensation of the organosilane molecules on the Si NPs surfaces. The suspension was washed several times in deionized water by centrifuging at 6000 rcf for 15 min to get rid of any excess APTES. Finally, the $-NH_2$ group-functionalized Si core NPs were redispersed in 28 mL of H_2O before use.

2.3. Gold Seeds. Colloidal gold solution 1−3 nm Au particles were prepared using THPC as the reductant according to Duff et al.[23] In short, 1.5 mL of 0.2 M NaOH was added to 45.5 mL of H_2O under rapid stirring, followed by the addition of 1 mL of 7×10^{-6} M aqueous THPC solution. After 2 min of stirring, 2 mL of 25 mM $HAuCl_4$ solution was added in one quick motion, after which the solution turn to dark brown color. The fast reaction is completed within 12 min. The final solution was kept in the refrigerator at 4.0 °C for at least 2 weeks before use.

2.4. Gold-Ion Plating Solution (K-gold). The gold plating solution, referred as K-gold, was obtained by dissolving 25 mg of K_2CO_3 in 100 mL of H_2O in a 125 mL flask, followed by the addition of 1.5 mL of 25 mM $HAuCl_4$. Under vigorous stirring, the solution turned transparent and colorless after 30 min, indicating the formation of gold hydroxide solution.

2.5. Si/Au Seeds. A 5 mL of the gold seeds (as prepared above) was added to a 4 mL aliquot of the Si NPs NH_2-functionalized suspension, and adhesion of the seeds on the amine-modified surface was added by lowering the pH under 3 with the addition of 2 mL of 1 M acetic acid. At this pH, the primary amines are protonated, thus allowing a higher yield and more homogeneous seed coverage. The solution was left to rest for 4 h. The excess of seeds was removed three times by centrifugation at 7000 rcf for 10 min, and the compound nanoparticles were redispersed in 3 mL of H_2O.

2.6. Shell Growth. To grow the gold shell, 5 mL of this matured K-gold solution was mixed with 3 mL of the Si/Au seeds NPs solution in a 20 mL vial. To order to study the PVP effect, 3 volumes are chosen as follows: without (denoted as core−islands heterostructures), with 50 μL (denoted as core−shell heterostructures), and with 70 μL (denoted as core−shell oligomer heterostructures) of an aqueous PVP 1.48 mM solution added to the mixture under vigorous stirring as a stabilizing agent for the resulting nanoshells, followed by 10 μL of formaldehyde (as a reducing agent) to reduce the unreacted gold ions. The nanoparticles were allowed to react 15 min before washing in water and centrifugation (7000 rcf, 15 min, 3 times) and finally redispersed in 3 mL of H_2O with a vortex.

2.7. Morphological Characterization. Field-emission scanning electron microscope (FE-SEM) has been done in a FEG system (Hitachi SU 8030 N) with the acceleration voltage of 5−10 kV to characterize the morphological properties of the different heterostructures. The SEM sample was prepared by dropping dispersion of heterostructures colloids on a silicon substrate to obtain the size distributions and the mean diameter, using the graphical software ImageJ. The dynamic light scattering (DLS) and ζ-potential were

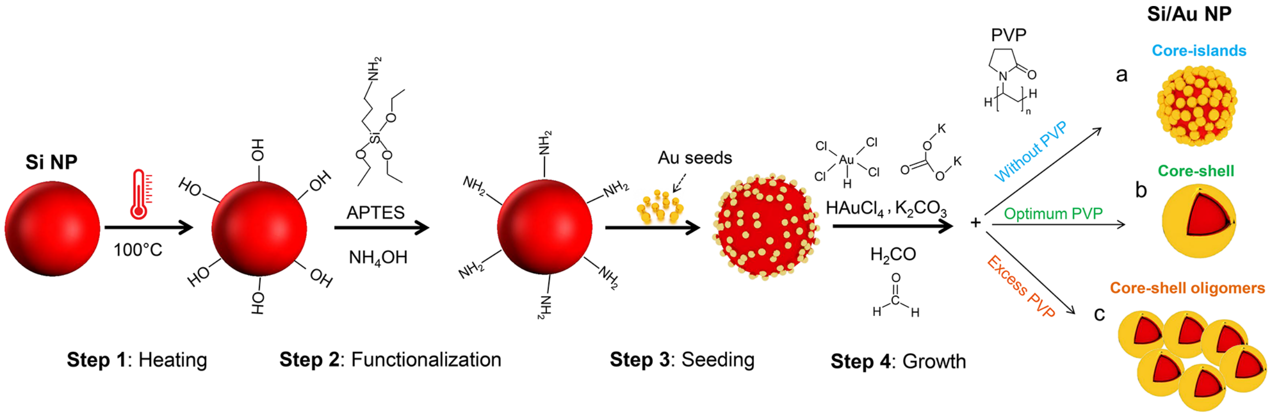

Figure 1. Schematic diagram showing the synthesis of Si/Au heterostructures. Step 1: Heating of silicon nanoparticle to create oxygen atoms surface termination. Step 2: Functionalization of the surface of Si NPs with NH_2-group. Step 3: Seeding of Au on the Si NPs surfaces. Step 4: Growth of the Au with different amounts of PVP with respect to its concentration. (a) Without PVP molecules, the core−islands heterostructure was obtained, (b) with optimum PVP molecules, the core−shell heterostructure was obtained, and (c) with an excess PVP molecules, the core−shell oligomer heterostructures were obtained.

measured on a Malvern Zetasizer Nano ZS in polystyrene cuvettes using 532 nm Nd:YAG laser opening at backscatter mode at an angle of 173° between sample and detector. The measurements were performed at room temperature. Errors bars correspond to the standard deviation from three measurements. The surface potential fitting model was the Smoluchowski approximation.

2.8. Optical Characterization. UV−visible extinction spectroscopy on solutions was performed on a Varian Cary 300 spectrophotometer in microquartz or polystyrene cuvettes with a path length of 1 cm over a wavelength range of 300 to 850 nm. A cuvette with deionized water was used as a reference for colloidal measurement.

Scattering spectra of individual nanoparticles were performed with a dark-field confocal microscope (Zeiss Axio Imager Z2). In backward-scattering geometry, a white lamp (Halogen 4100K, Philips) was focused on the sample using a 50× dark field objective (numerical aperture, NA = 0.8−0.95, Zeiss) to illuminate a single nanoparticle, which led to the angle of light incidence in the range from 53.1° to 71.8° with respect to the normal to the glass substrate. The collection of the signal was performed by the same objective with NA = 0.8. The collected light is filtered confocally using an optical fiber coupled to a lens. The fiber has a 50 μm core size and the collection zone corresponds to 3 μm on the substrate. It is connected to the spectrometer Ocean Optics QE65000. Color scattering images were captured using a color digital camera (Zeiss) mounted onto the imaging plane of the microscope.

2.9. UV Photolithography. To locate position of the nanoparticles, we have developed a grid mesh on a glass substrate by UV photolithography technique. We use photoresists S1813 with under-cut structures by mask aligner MJB4 (Suss MicroTec). Finally, the residual photoresist could be removed by acetone and sonication.

2.10. Numerical Simulations. The scattering cross-section spectra and electric and magnetic near-fields distributions were calculated with analytic Mie theory and finite-difference time-domain (FDTD) methods. In FDTD model, the total-field scattered-field (TFSF) source was used to realize the plane wave incidence. The boundary conditions of the perfectly matched layer (PML) were applied, and the three-dimensional sizes were set as 2 μm × 2 μm × 2 μm. A nonuniform mesh with the smallest size of 0.5 nm as well as a perfectly matched boundary was employed in the numerical simulations. The dielectric function of silicon and silica were taken from the material database of Palik[24] (provided by FDTD Solutions, Lumerical). Data from Johnson and Christy[25] is used for the dielectric constant of gold.

3. RESULTS AND DISCUSSION

3.1. Synthesis of Si/Au Heterostructures. Our fine synthesis control of the size and coverage of Au nanoparticles on the surface of Si NPs represents a crucial step for tailoring their coupling hybridization plasmon.[26] The strategy used to synthesize the Si/Au heterostructures with different geometries is illustrated in Figure 1. The most important step of our synthesis method is already published for SiO_2/Au core−shell nanoparticles.[27,28] Thus, the complete procedure can be divided into four steps: (i) heating of Si nanoparticles to hydrolyze the surface, (ii) the functionalization of the silicon nanoparticles with amine groups, (iii) binding of Au seeds onto the surface of the Si NP, and finally (iv) the gold shell growth. The details of the synthesis are presented in the Experimental Section. The Si nanoparticles have been mechanically fabricated using a blender, as reported in our previous work.[5]

During the growth of the gold shell, we demonstrate that the presence of nonionic PVP surfactant in the colloidal solution could significantly influence the distribution of Au on the Si nanoparticles. The value of the ζ-potential of the Si NPs is −23 mV. This value increases to +5 mV after the functionalization process by APTES. The positive charge indicates the presence of NH_2 group. Then, there is a decrease to −33 mV as the Au seeds attached to the NPs. All results of ζ-potential of the Si/Au heterostructures nanoparticles are shown in Table S1. Furthermore, the ζ-potential of Au seeds was measured separately and found to be −40 mV (Figure S1b), which confirmed the attachment of Au seeds at the surface of Si NPs. The all negative charge measured from Au seeds and the Si/Au heterostructures originated from the capping molecules of Au seeds or the formation of gold layer. The THPC-induced gold seeds (1−3 nm) exhibited a negative charge in the range of −40 to −45 mV.[29,30] These negatively charged Au seeds induce the negative charge measured for Si/Au core−islands

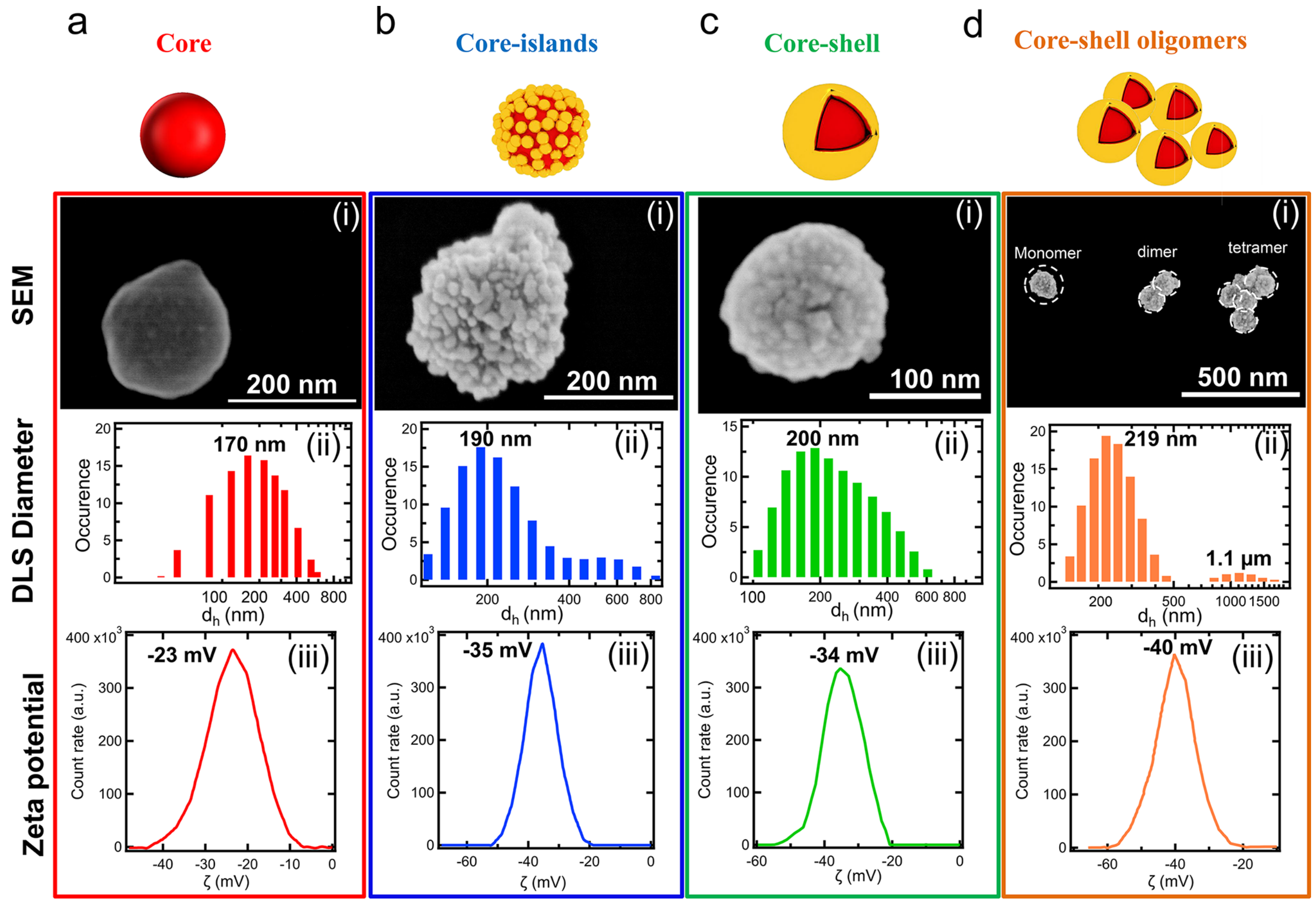

Figure 2. Four different structures: pristine Si core and different Si/Au heterostructures. (Top panels, a(i)−d(i)) SEM images, (middle panels, a(ii)−d(ii)) hydrodynamic diameter (d_h) distributions via dynamic light scattering (DLS) (bottom panels, a(iii)−d(iii)) and ζ-potential of each structure. The colors borders in parts a−d denote the name of structures: pristine Si core (red) and Si/Au core−islands (blue) and Si/Au core−shell (green) and Si/Au core−shell oligomers (orange) heterostructures. In the inset of part d(i), the typical monomer, dimer and tetramer of Si/Au core−shell oligomers are marked with white dashed lines. All values shown in the DLS diameter and the ζ potential are the average values.

nanostructures. Moreover, the complete growth of the Au shell onto the Si nanoparticles results in the same negative charge.[31]

Depending on the amounts of PVP molecules added in the suspension in the step 4 (see Figure 1); the growth mechanism resulted in three different structures labeled as (a) core−islands, (b) core−shell, and (c) core−shell oligomers Si/Au heterostructures.

3.1.1. Synthesis of the Si/Au Core−Islands Heterostructures. The morphology of obtained heterostructures was characterized by scanning electron microscopy (SEM), as shown in the Figure 2b(i). SEM image shows that the gold islands were found to nucleate on silicon surface, and grown with random orientations with the respect to the surface. The hydrodynamic diameter (d_h) distributions through a solution of Si/Au core−islands NPs is characterized by dynamic light scattering (DLS) measurements (Figure 2b(ii). The average d_h value increases from 170 nm for Si NPs to 190 nm when the Au satellites decorate the Si NPs surfaces. From the difference between these mean d_h values, the average size of Au islands could be roughly evaluated as about 10 nm. To confirm this average size from SEM images, we performed a statistical analysis using imageJ software on several nanoparticles, as shown in Figure S2).

In addition, the effects of the metal ion doping on the surface charge were characterized by the ζ-potential measurement (Figure 2b(iii). The surface is negatively charged with value of ζ = −35 mV with low dispersion as the gold islands grown on the surface of Si nanoparticles. This value is sufficient to prevent any interactions between the NPs and therefore maintains the stability of the solution.[32]

3.1.2. Synthesis of the Si/Au Core−Shell Heterostructures. In previous section, we demonstrated the Au decoration on the Si-NPs. Here, we studied the influence of the addition of a nonionic surfactant as stabilizing agent, such as PVP, on the growth of the Au shell on Si NPs. Briefly, we repeat the same protocol used in the synthesis of the core−islands heterostructure, but we added a small amount of PVP in the colloidal solution during the growth of the Au shell (see Figure 1, step 4). We added 10 µL of pure formaldehyde in a solution containing 3 mL of Si NPs decorated with Au seeds (25 mM), 50 µL of PVP (1.48 mM), and 5 mL of K-gold (see Experimental Section). We finally obtained Si/Au hybrid NPs as shown on Figure 2c. We measured the average hydrodynamic diameter d_h to be equal to 200 nm, as shown in Figure 2c(ii). Comparing with the d_h value measured for the bare Si NPs, the average thickness Au shell could be estimated to be 15 nm. Furthermore, the ζ-potential of Si/Au core−shell heterostructure shows that the NP surface is negatively charged showing a value of −34 mV (Figure 2c(iii)), allowing a good stability in time.

3.1.3. Synthesis of the Si/Au Core−Shell Oligomers Heterostructures. As demonstrated above, the presence of a small amount of PVP allows us to obtain Si/Au core−shell heterostructures. Here, we report the effect of an increase of the PVP concentration (up to 70 μL at 1.48 mM) during the Au growth step (Step 4). Figure 2d(i) shows the SEM image of resulting nanostructures. It appears that multimers are made of smaller nanoparticles, such as dimers, tetramers, and other arbitrary oligomers. Moreover, the biggest Si/Au core−shell nanoparticles are not showing any agglomeration (SEM images not shown here). The agglomeration of the smallest particles is due to the short length of PVP (molecular weight of 10 000 g/mol) used in our work, while the longer length PVP is already known to prevent the agglomeration of nanoparticles.[33] This observation is confirmed by the DLS measurements. Indeed, we observed two nanoparticle size distributions, and their average d_h values are 219 nm (increasing of Au shell thickness) and 1.1 μm for oligomers. However, the ζ-potential of Si/Au core−shell oligomers heterostructures nanoparticles shows a value of −40 mV (Figure 2d(iii)).

In the following, we address the close correlation between the different obtained heterostructures and their optical responses.

3.2. Optical Properties. *3.2.1. UV−Vis Colloidal Characterization.* To verify the optical properties in Si/Au heterostructures, UV−vis extinction spectroscopy of the colloidal solutions was first used to characterize the pristine Si core and the different Si/Au heterostructures. The solution color of the pristine Si core and Si/Au heterostructures suspensions changes from light-brown (Si core) to blue when the Au coverage on the Si NPs surfaces, as shown in Figure 3a. Figure 3b shows the normalized extinction spectra for the various Si/Au heterostructures (core−islands high coverage, core−shell, core−shell oligomers), whereas the extinction spectrum of the pristine Si NPs core was shown for comparison with them.

For all the different hybrid structures Si/Au, a significant modification of the extinction spectra was obtained. The extinction spectrum of the pristine colloidal Si NPs (red curve) shows a broad band ranging from ultraviolet (UV) to near-infrared (NIR) with a maximum peak at 400 nm (see Figure 3b), consistent with previous reports.[5,34,35] The broadening of the extinction peak was attributed to wide size distribution of Si NPs. Moreover, when Au NPs are grafted onto the Si NPs, the extinction spectrum dramatically changes and shows a splitting into two plasmon bands at low and high wavelengths.[36,37] This phenomenon is known as plasmon hybridization. First, the position of the peak at low-wavelength 400 nm is unchanged for the different heterostructures. On the other hand, the plasmon bands at high-wavelength present two peaks for Si/Au core−islands heterostructures (blue curve). The first one located at 540 nm corresponds to a dipolar mode of gold structures, and the second one located at 620 nm corresponds to a dipolar mode of the Si/Au core−shell, where both peaks exhibit a redshift and a broadening of the extinction spectra as the shape of Si/Au heterostructures changed from core−islands to core−shell and then to core−shell oligomer nanoparticles. These results are correlated to an increase of Au shell thickness around the Si NPs core, in good agreement with above results of SEM images and DLS measurements shown Figure 2.

3.2.2. Single-Particle Scattering Properties of Si/Au Heterostructures. Single-particle dark-field scattering spectroscopy was used to measure the scattering spectra of the different hybrid nanoparticles. All heterostructures were prepared by drop-casting of 1 μL of diluted colloidal solution onto a glass substrate engraved with a grid. The substrate grid mesh fabricated via photolithographic technique was used to correlate the SEM of each heterostructure with its scattering spectrum according to the procedure defined in our previous work.[5]

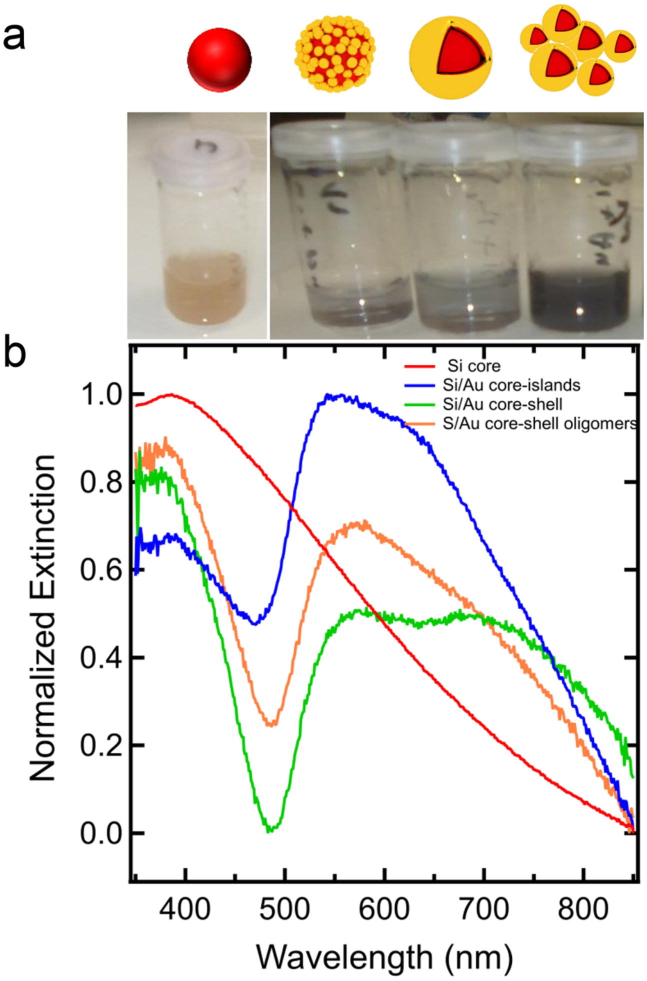

Figure 3. Extinction properties in solution. (a, top) Schemes of the pristine Si core, the Si/Au core−islands, the core−shell. and the core−shell oligomers heterostructures. (a, bottom) Photographs of the corresponding colloidal solutions. (b) UV−vis normalized extinction spectra of the colloidal solutions.

3.2.2.1. Pristine Si Core. Parts a and b of Figure 4 show the SEM image and the measured backward dark-field scattering spectrum of a typical Si NP of 120 nm in diameter. It can be seen from the SEM analysis via ImageJ software that the nanoparticle presents a quasi spherical shape with circularity factor of f = 97%. The measured scattering spectrum exhibits two peaks at 461 and 525 nm with almost same magnitude (Figure 4b). The two resonances modes are thus assigned to the electric dipole (ED) and magnetic dipole (MD) Mie resonances.[5,38,39] We simulated the scattering cross-section (C_{sca}) spectrum of the Si NP on a glass substrate using FDTD method (Lumerical Solutions, Inc. 8.15) with a diameter of 120 nm, as measured by SEM. We consider a 2 nm thick SiO_2 layer on the nanoparticle coming from the native oxide, as shown in Figure 4c. Two resonance modes were observed at 430 and 510 nm and are theoretically assigned to the electric and magnetic dipole modes, respectively.[5,6,34] Moreover, as is

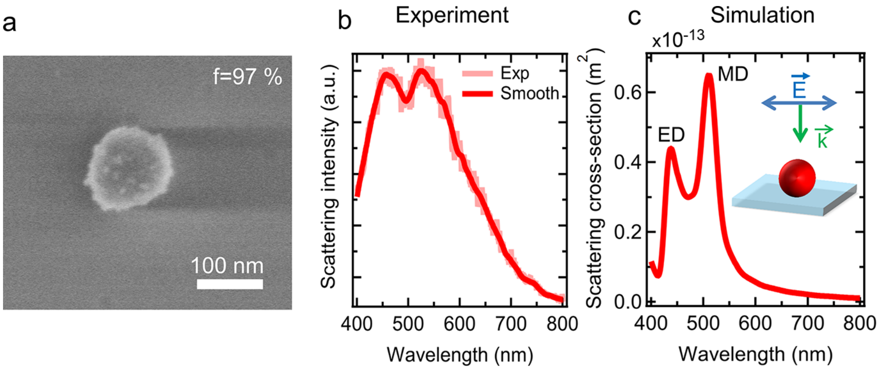

Figure 4. Scattering properties of the pristine Si NP. (a) SEM image of the fabricated Si NP. (b) Measured and (c) FDTD-simulated scattering cross-section spectrum of the Si NP with diameter of 120 nm including a SiO_2 shell of 2 nm in thickness. The measured scattering spectrum is smoothed using a Savitzky–Golay filter to reduce the instrumental noise. Inset of part a shows the percent number indicate the circularity factor determined using ImageJ software. Inset of part c shows the schematic of the Si NP placed on a glass substrate under light illumination from the top used for FDTD simulation in this study.

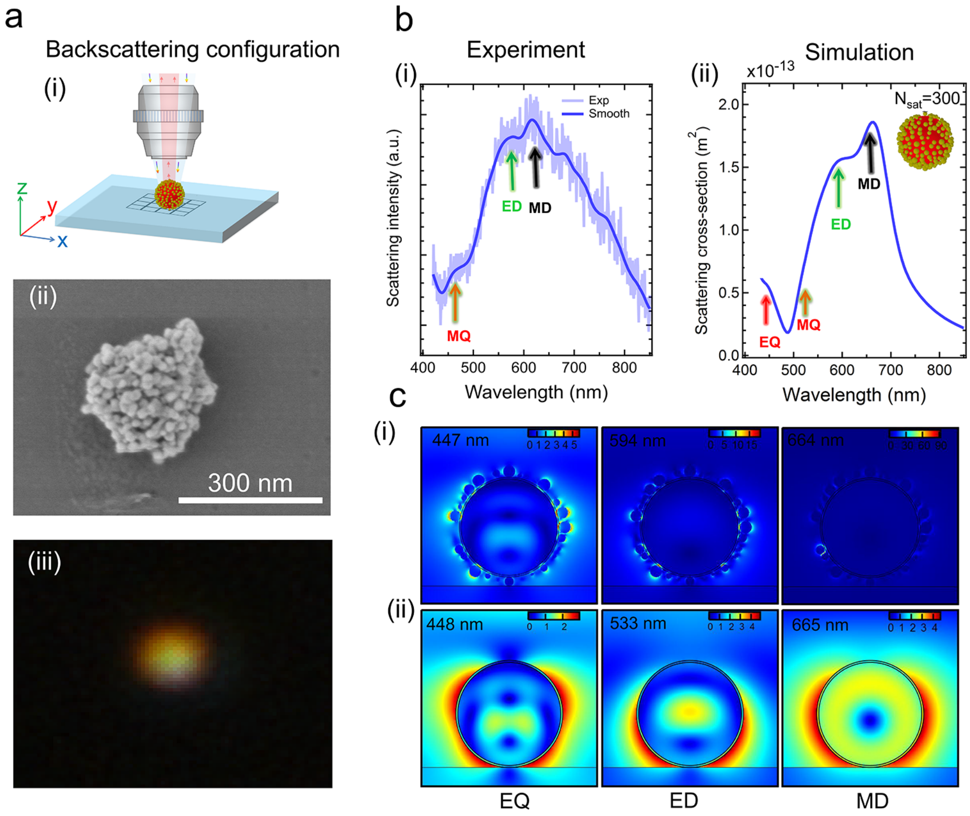

Figure 5. Scattering properties of the Si/Au core–satellites heterostructure. (a) 3D scheme of the dark-field illumination and backward scattering collection measurement geometry (i), SEM (ii) and dark-field (iii) images. (b) Measured (i) and FDTD-simulated (ii) scattering spectra of the core–satellites heterostructure. Measured scattering spectrum is smoothed via Savitzky-Golay filter to reduce instrumental noise. Inset of part b(ii) shows the scheme of the core–satellites heterostructure with 300 satellites used in our simulations. (c) FDTD simulated of the electric near-field distributions in the *xz* plane at different excitation wavelengths of the core–satellites heterostructure (i) compared with the pristine Si core (ii). In the both heterostructures case, a 3 nm thick SiO_2 layer around Si core is taken into account in the simulations. For more clarity, the electric near-field distributions was plotted in a logarithmic scale only in part c(i).

well-known, the nonideal spherical shape of NP affects the magnitude of both magnetic and electric dipole modes.[5,6] The simulated scattering spectrum shows a good agreement with the measured one, though some slight differences in magnitude of resonance modes exist, which is discussed in our previous work.[5] As the nanoparticle diameter increases, these peaks shift toward longer wavelengths and become broad. Then additional resonances appear attributed theoretically to magnetic quadrupolar (MQ) and electric quadrupolar (EQ) modes, and then higher orders of resonances appear as still more increasing of the diameter.[5]

Therefore, we focus on the scattering properties of single Si/Au hybrid NPs with different geometries: core–islands, core–shell, and core–shell oligomer measured through single-particle dark-field spectroscopy.

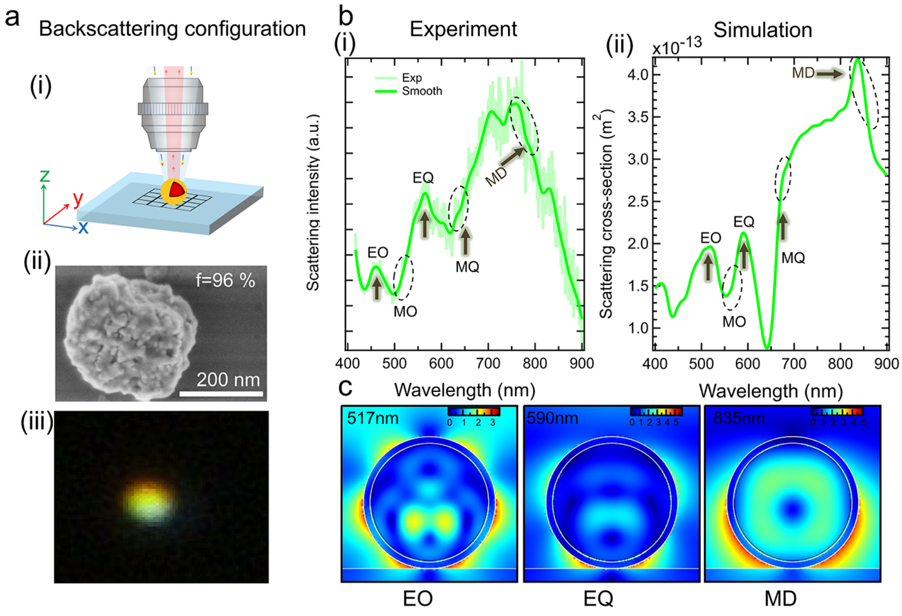

Figure 6. Scattering properties of the Si/Au core−shell heterostructure. (a) 3D scheme of dark-field illumination and backward scattering collection measurement geometry (i), SEM image (ii), and dark-field images (iii). (b) Measured (i) and FDTD simulated (ii) scattering spectra of the Si/Au core−shell heterostructure. Measured scattering spectrum is smoothed via Savitzky-Golay filter to reduce instrumental noise. The dashed circles represents the Fano lineshapes. (c) FDTD simulation of the electric near-field ($|E|/|E_0|$) distributions in the *xz* plane at different excitation wavelengths. Inset of part a(ii) in the top right corner is the percent number indicating the circularity factor.

3.2.2.2. Core−Islands Heterostructure. The scattering spectrum of the core−islands heterostructure is measured via a backward scattering configuration confocal microscope, as shown in Figure 5a(i). The size of the NP was determined from the SEM image (Figure 5a(ii)) using ImageJ software. Thus, the total particle diameter is 195 nm, and the Au islands are in random position and have nonuniform diameters ranging from 10 to 25 nm with an average diameter of $d_{sat} \simeq 14$ nm (Figure S2b). Considering the above measurements, the Si core diameter is estimated to be $d_c \simeq 170$ nm. Figure 5a(iii) shows the dark-field image, showing a red color. Figure 5b(i) shows the measured and smoothed scattering spectra. Because of the difficulty to simulate the scattering spectrum of the exact morphological core−islands heterostructure, we assumed that the Si core is decorated by Au satellites nonuniform in size and randomly distributed in position. Figure S3 shows the calculation of the scattering cross-section spectra as a function of Au satellites on the Si core. In order to mimic the real morphology of the considered NP, FDTD simulations were performed on core−satellite assemblies with an increasing number of satellites (i.e., from 0 to 230) randomly positioned on the Si core and presenting a distribution in size[37,40] and taking into account a 3 nm thick SiO_2 layer around the Si nanoparticle. We consider that a thickness of 3 nm of SiO_2 capped the Si NPs in our simulations. This thickness coming from the oxidation processes is explained in the Experimental Section: 2 nm coming from the native oxide of silicon NPs[5] and 1 nm coming from heating step of silicon NPs to 100 °C in the first step of the synthesis of Si/Au heterostructures (Figure 1). The different observed peak resonances are identified by arrows in both measured and simulated scattering spectra.

Overall, experimental and simulated scattering spectra agree well with slight differences. Indeed, the widths of experimental peaks are often broader and the peak positions are slightly shifted. The differences are attributed to simplifications mode in our simulations: (i) the number and distribution of Au islands decorating the Si NP surface, (ii) the nonspherical shape of Si core nanoparticle,[5] and (iii) incomplete collection of the scattering light (NA = 0.8) of the collection objective.[41]

In order to interpret the modes associated with the scattering peaks, maps of electric near-field distributions at corresponding excitation wavelengths (447, 594, and 664 nm) are calculated, as shown in Figure 5c(i). It is apparent that the near-field enhancement for different excitation wavelengths are confined at the satellites-core interfaces, thus inducing hot spots in the silica spacer. This is attributed to the fact that the dipole moments of the Au satellites are more easily excited by the incident electric field.[37,42]

On the other hand, at MD mode wavelength, the field enhancement dominates between the satellites revealing a collective magnetic dipolar mode.[40,43−45] For comparison, we show in Figure 5c(ii) the near-field distributions of Si nanoparticle of 170 nm in diameter including a 3 nm thick SiO_2 shell. It clearly appears that the near-field distribution dramatically changes with the presence of Au particles at the Si core surface.

To confirm this analysis, electric dipolar and quadrupolar modes are clearly identified via the surface charge density distributions (Figure S4). For both modes, the dipole moments of Au satellites are perpendicular to the Si NP surface. However, for the magnetic dipolar mode, the dipole moments of Au satellites are parallel to the Si NP surface and create a circular displacement current that induced a collective magnetic dipolar mode.[40,43−45] We conclude from this analysis that the excitation and the nature for different modes of Au satellites are caused by two main mechanisms. First, the excitation comes from the incident electromagnetic (EM) field that excites the Au satellites on the Si NPs. Second, a strong field near the outer surface is associated with the hot spots that exist for the localized surface plasmon of the Au satellites located in the region.[46] Results indicate that the strongly enhanced electric field is attributed to the Si NPs and the localized surface plasmon resonance of the Au satellites coupling.

3.2.2.3. Core−Shell Heterostructure. Here we report the scattering properties of the Si/Au core−shell heterostructures. Figure 6a(i) shows a scheme of the dark-field (backward) scattering measurement. Parts (ii) and (iii) of Figure 6a show the SEM and dark-field images, respectively. SEM analysis shows that the shape is quasispherical with a circularity factor of 96% and a total diameter of about 300 nm. Furthermore, the dark-field scattering image reveals that the Si/Au core−shell heterostructure scatters a yellow-green color. The measured scattering spectrum shows multiple peaks, as shown in Figure 6b(i). Using FDTD simulation and the total diameter size measured by SEM, we estimated the shell thickness by adjusting the simulated to the measured scattering spectrum. Thus, considering a 3 nm thick SiO_2 layer around the Si core, the best agreement is obtaining for a 15 nm thick Au shell. Furthermore, the gold thickness is consistent with DLS measurements (Figure 2c(ii)), where the measured average hydrodynamic diameter d_h in solution increased from 170 nm for pristine Si core to 200 nm for core−shell heterostructure.

To further ascertain the origins of the peaks, we decomposed the scattering efficiency into different multipolar contributions of the Si/Au core−shell NPs with radius $[r_1, r_2]$ = [135, 150] nm in free space using the Mie theory,[47] as shown in Figure S5. Then, we attribute the peaks observed at 835 nm to the magnetic dipolar (MD) mode, at 675 nm to the magnetic quadrupolar (MQ), and at 570 nm to the magnetic octupolar (MO) of the Si core, whereas the other resonances wavelengths observed at 590 nm and at 517 nm are attributed to the electric quadrupolar (EQ) and the electric octupolar (EO) modes, respectively.[20] Furthermore, FDTD simulations of electric near-field distributions of the Si/Au core−shell were performed at these different excitation wavelengths, confirming their origins.

The comparison between experiment-simulation shows some differences such as the slight peak blue shift wavelength and the broadening of the line width of each mode. These differences arise from the nonisotropic scattering induced by the not perfect spherical shape of NP, clearly observed on the dark field scattering image (Figure 6a(iii)).

Additionally, multiple Fano lineshapes are clearly observed, which are marked by dashed circles in both measured and calculated scattering spectra in Figures 6b(i) and 7a, respectively.

To understand the singularities and the asymmetric profile observed in the experimental scattering spectrum (Figure 6b(i), the scattering, the absorption cross-section, and the near-field distributions were separately calculated in wide wavelength range using the FDTD method. We used the experimental parameter in our simulation (nanoparticle dimensions, the NP connected with the SiO_2 substrate, the top backscattering light collection). These results clearly demonstrate that the Si/Au exhibits well-pronounced Fano resonances with strong suppression of the scattering cross-section in the different orders. The peaks are identified according the above decomposition into multipolar contributions (Figure S5).[15,16] It can be noted that the electric and magnetic dipolar Fano lineshapes are more visible than the quadrupolar Fano lineshapes. The asymmetric profile observed in the scattering cross-section of magnetic dipolar and quadrupolar Fano resonances result from the interference between the sharp magnetic dipole (MD) and the magnetic quadrupole (MQ) of the Si core and the broad electric dipole of Si/Au core−shell. Moreover, we calculated the electric and magnetic near-field distributions at selected Fano resonance wavelengths, as shown in Figure 7b. Thus, the calculations clearly show that the field distributions correspond to the (a_1, ED), (a_2, EQ), (b_1, MD), (b_2, MQ), and (b_3, MO), respectively.

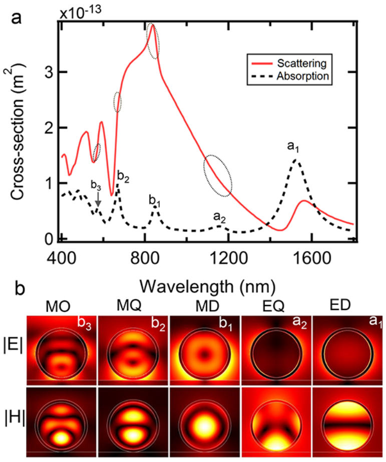

Figure 7. Fano resonances. (a) FDTD simulated of scattering (red solid line) and absorption (black dashed line) cross-section in wide-range wavelengths [400:1800] nm of the Si/Au core−shell heterostrcuture. (b) Electric (top panel) and magnetic (bottom panel) near-field distributions in the *xz* plane at different Fano resonances excitation wavelengths. a_1 and a_2 are the electric dipolar and quadrupolar Fano resonance modes and b_1, b_2, and b_3 are the magnetic dipolar, quadrupolar, and octupolar Fano resonance modes associated with the Mie scattering coefficients.

Since the Si NPs are fabricated by a mechanical method, it is possible to found other shapes of Si/Au core−shell heterostructures (e.g., oblate ellipsoid). Their detailed scattering properties study is shown in Figures S6 and S7.

3.2.2.4. Core−Shell Oligomer Heterostructure. Figures 8a(i−iii) show the 3D scheme of backward scattering measurement configuration geometry, the SEM, and the dark-field images of the Si/Au core−shell oligomer heterostructures, respectively. SEM analysis shows that the core−shell nanoparticles agglomerate and that each nanoparticle presents a quasi spherical shape. The diameter of each nanoparticle has been determined directly from SEM image using ImageJ software, whereas the Si core diameters and the thick Au shell are estimated by adjusting the measured to simulated scattering spectra. Converting to the previous cases, it can be seen that the measured scattering spectrum does not present strong singularities, as shown in the Figure 8b(i). Then, FDTD simulation of scattering spectrum was performed. A good agreement between the measured and the simulated scattering spectra was obtained. Thus, the best set of size parameters (R_{Si}, t_{SiO2}, t_{Au}) allowing one to calculate the scattering cross section is shown in Table S2.

To understand the interactions of EM field with the Si/Au core−shell oligomer heterostructures, we simulated the electric near-field distributions at different wavelengths in the *xy* plane at z = 55 nm, as shown in Figure 8c. First, at low wavelengths (466 and 503 nm), it clearly appears that a strong enhancement of the electric field exists in the gaps between particles. On the other hand, at the longest wavelength (673

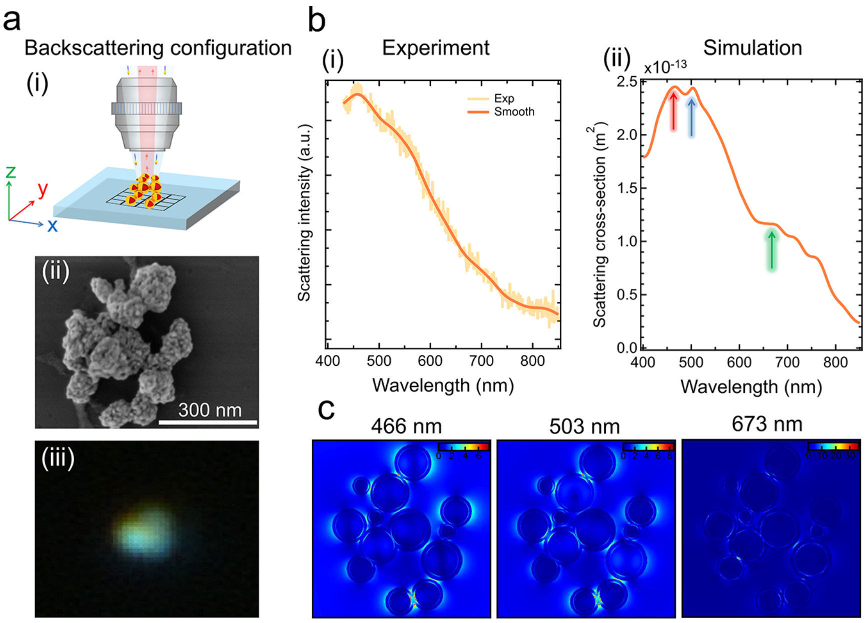

Figure 8. Scattering properties of the Si/Au core−shell oligomer heterostructures. (a) Schematic illustration of dark-field backscattering measurement geometry (i), SEM (ii), and dark-field (iii) images. (b) Measured and FDTD simulated scattering spectra of the core−shell oligomer heterostructures. Measured scattering spectrum is smoothed via Savitzky-Golay filter to reduce instrumental noise. (c) FDTD simulated of the electric near-field distributions in a logarithmic scale at different excitation wavelengths in the *xy* plane at $z = 55$ nm.

nm), the electric field is mainly confined in the silica layer in each Si/SiO_2/Au particle. For this heterostructures, we cannot observe the Fano resonance compared to above Si/Au core−shell heterostructure, which may be attributed to unordered oligomers.

4. CONCLUSIONS

In summary, we have reported, for the first time, on the synthesis of the dielectric−metal Si/Au colloidal heterostructures through a combination of both mechanical and chemicals methods. By varying the amount of PVP molecules respect to its concentration, three heterostructures have been found, such as Si/Au core−islands, Si/Au core−shell, and Si/Au core−shell oligomers. The optical properties of these different heterostructures have been investigated. Compared with the pristine Si core, the UV−vis extinction spectra of the various heterostructures exhibit a splitting of two bands in visible and NIR regions that is attributed to hybridization plasmon. Thanks to photolithographic and drop-cast deposition of colloid nanoparticles on the glass substrate, we experimentally investigated the single-particle dark-field scattering properties of the different heterostructures. To more understand these results, we have investigated to the FDTD simulations of the scattering spectra and of the electric near-field distributions for the various heterostructures. As for the Au-decorated Si core, the scattering spectrum is dominated by the collective magnetic dipole due to light coupling Au islands, while for the Au-coated Si nanoparticle, the hybridization plasmon with Fano lineshapes has been clearly observed. Finally, the scattering spectra of the Si/Au core−shell oligomer heterostructures are very flat. Our synthesis method can be applied to form a diverse range of Si-metal heterostructures for tailored applications.

■ ASSOCIATED CONTENT

Supporting Information

The Supporting Information is available free of charge at https://pubs.acs.org/doi/10.1021/acs.jpcc.1c06182.

> Gold seeds, basic colloidal characterization of heterostructures, SEM images of the Si/Au core−islands heterostructure, satellites decorated number effect on scattering properties of the Si core, surface charge density distribution of the core−satellites heterostructures, decomposition modes of scattering properties of the Si/Au core−shell, scattering of the core−shell oblate heterostructures, size parameters of the Si/Au core−shell oligomer heterostructures, and scattering spectrum of the Si/Au core−shell oligomer heterostructure (PDF)

■ AUTHOR INFORMATION

Corresponding Authors

Julien Proust − *Light, nanomaterials, nanotechnologies (L2n) Laboratory, CNRS ERL 7004, University of Technology of Troyes, F-10004 Troyes Cedex, France;* orcid.org/0000-0001-6375-4027; Email: julien.proust@utt.fr

Jérôme Plain − *Light, nanomaterials, nanotechnologies (L2n) Laboratory, CNRS ERL 7004, University of Technology of Troyes, F-10004 Troyes Cedex, France;* orcid.org/0000-0001-5806-9965; Email: jerome.plain@utt.fr

Authors

Wajdi Chaâbani − *Light, nanomaterials, nanotechnologies (L2n) Laboratory, CNRS ERL 7004, University of Technology of Troyes, F-10004 Troyes Cedex, France; Laboratoire de Physique-Mathématiques et Applications, Faculté des Sciences de Sfax, Université de Sfax, 3000 Sfax, Tunisia;* orcid.org/0000-0003-1077-2752

Samuel Ouellet − *Light, nanomaterials, nanotechnologies (L2n) Laboratory, CNRS ERL 7004, University of Technology of Troyes, F-10004 Troyes Cedex, France; Centre* *d'optique, Photonique et Laser, Université Laval, Québec, Québec G1 V 0A6, Canada*

Artur Movsesyan − *Light, nanomaterials, nanotechnologies (L2n) Laboratory, CNRS ERL 7004, University of Technology of Troyes, F-10004 Troyes Cedex, France;* orcid.org/0000-0002-5425-7747

Jérémie Béal − *Light, nanomaterials, nanotechnologies (L2n) Laboratory, CNRS ERL 7004, University of Technology of Troyes, F-10004 Troyes Cedex, France*

Renaud Bachelot − *Light, nanomaterials, nanotechnologies (L2n) Laboratory, CNRS ERL 7004, University of Technology of Troyes, F-10004 Troyes Cedex, France;* orcid.org/0000-0003-1847-5787

Tao Xu − *School of Mechatronic Engineering and Automation, Key Laboratory of Advanced Display and System Applications, Ministry of Education, Shanghai University, 200072 Shanghai, China*

Anne-Laure Baudrion − *Light, nanomaterials, nanotechnologies (L2n) Laboratory, CNRS ERL 7004, University of Technology of Troyes, F-10004 Troyes Cedex, France;* orcid.org/0000-0001-9751-9957

Pierre-Michel Adam − *Light, nanomaterials, nanotechnologies (L2n) Laboratory, CNRS ERL 7004, University of Technology of Troyes, F-10004 Troyes Cedex, France;* orcid.org/0000-0003-3065-9394

Denis Boudreau − *Centre d'optique, Photonique et Laser, Université Laval, Québec, Québec G1 V 0A6, Canada;* orcid.org/0000-0001-5152-2464

Abdallah Chehaidar − *Laboratoire de Physique-Mathématiques et Applications, Faculté des Sciences de Sfax, Université de Sfax, 3000 Sfax, Tunisia;* orcid.org/0000-0001-5372-2646

Complete contact information is available at:
https://pubs.acs.org/10.1021/acs.jpcc.1c06182

Notes

The authors declare no competing financial interest.

ACKNOWLEDGMENTS

Financial support of Nano'Mat (www.nanomat.eu) by the Ministère de l'enseignement supérieure et de la recherche, the Labex Action, the "Fonds Européen de Développement Régional (FEDER) fund", the "region Grand-Est", and the "Conseil général de l'Aube" are acknowledged. Parts of this project were supported by the Tunisia Alternation Scholarship, the Fondation UTT, and the Agence nationale de la recherche (ANR), Contract NATO (ANR-13-BS10-0013). This work has been supported by the EIPHI Graduate School (Contract "ANR-17-EuRE-0002"). This work has been made within the framework of the Graduate School NANO- PHOT (École Universitaire de Recherche, contract ANR-18-EURE-0013).

REFERENCES

(1) Besteiro, L. V.; Yu, P.; Wang, Z.; Holleitner, A. W.; Hartland, G. V.; Wiederrecht, G. P.; Govorov, A. O. The Fast and the Furious: Ultrafast Hot Electrons in Plasmonic Metastructures. Size and Structure Matter. *Nano Today* **2019**, *27*, 120−145.

(2) Zhou, N.; López-Puente, V.; Wang, Q.; Polavarapu, L.; Pastoriza-Santos, I.; Xu, Q.-H. Plasmon-Enhanced Light Harvesting: Applications in Enhanced Photocatalysis, Photodynamic Therapy and Photovoltaics. *RSC Adv.* **2015**, *5*, 29076−29097.

(3) Mayer, K. M.; Hafner, J. H. Localized Surface Plasmon Resonance Sensors. *Chem. Rev.* **2011**, *111*, 3828−3857.

(4) Baffou, G.; Quidant, R. Thermo-plasmonics: using Metallic Nanostructures as Nano-Sources of Heat. *Laser Photonics Rev.* **2013**, *7*, 171−187.

(5) Chaabani, W.; Proust, J.; Movsesyan, A.; Beal, J.; Baudrion, A.-L.; Adam, P.-M.; Chehaidar, A.; Plain, J. Large-Scale and Low-Cost Fabrication of the Silicon Mie resonators. *ACS Nano* **2019**, *13*, 4199−4208.

(6) Kuznetsov, A. I.; Miroshnichenko, A. E.; Fu, Y. H.; Zhang, J.; Luk'yanchuk, B. Magnetic Light. *Sci. Rep.* **2012**, *2*, 492.

(7) Tsuchimoto, Y.; Yano, T.; Hayashi, T.; Hara, M. Fano Resonant All-Dielectric Core/Shell Nanoparticles with Ultrahigh Scattering Directionality in the Visible Region. *Opt. Express* **2016**, *24*, 14451−14462.

(8) Yan, J.; Liu, P.; Lin, Z.; Wang, H.; Chen, H.; Wang, C.; Yang, G. Directional Fano Resonance in a Silicon Nanosphere Dimer. *ACS Nano* **2015**, *9*, 2968−2980.

(9) Miroshnichenko, A. E.; Kivshar, Y. S. Fano Resonances in All-Dielectric Oligomers. *Nano Lett.* **2012**, *12*, 6459−6463.

(10) Yan, J. H.; Liu, P.; Lin, Z. Y.; Wang, H.; Chen, H. J.; Wang, C. X.; Yang, G. W. Magnetically Induced Forward Scattering at Visible Wavelengths in Silicon Nanosphere Oligomers. *Nat. Commun.* **2015**, *6*, 7042.

(11) Sugimoto, H.; Fujii, M. Broadband Dielectric−Metal Hybrid Nanoantenna: Silicon Nanoparticle on a Mirror. *ACS Photonics* **2018**, *5*, 1986−1993.

(12) Feng, T.; Xiang, J.; Zhang, C.; Liang, Z.; Xu, Y. Ultrathin Conductive Coating Effects on the Magnetic and Electric Resonances of Silicon Nanoparticles. *J. Opt. Soc. Am. B* **2017**, *34*, 653−657.

(13) Feng, T.; Xu, Y.; Zhang, W.; Miroshnichenko, A. E. Ideal Magnetic Dipole Scattering. *Phys. Rev. Lett.* **2017**, *118*, 173901.

(14) Yang, Z.-J.; Zhao, Q.; Deng, Y.-H.; Zhang, D.; He, J. Efficient second harmonic generation in gold/silicon core/shell nanostructures. *Opt. Express* **2018**, *26*, 5835−5844.

(15) Miroshnichenko, A. E. Off-Resonance Field Enhancement by Spherical Nanoshells. *Phys. Rev. A: At., Mol., Opt. Phys.* **2010**, *81*, 053818.

(16) Sancho-Parramon, J.; Jelovina, D. Boosting Fano Resonances in Single Layered Concentric Core−Shell Particles. *Nanoscale* **2014**, *6*, 13555−13564.

(17) Liu, P.; Chen, H.; Wang, H.; Yan, J.; Lin, Z.; Yang, G. Fabrication of Si/Au Core/Shell Nanoplasmonic Structures with Ultrasensitive Surface-Enhanced Raman Scattering for Monolayer Molecule Detection. *J. Phys. Chem. C* **2015**, *119*, 1234−1246.

(18) Kutrovskaya, S.; Arakelian, S.; Kucherik, A.; Osipov, A.; Evlyukhin, A.; Kavokin, A. V. The Synthesis of Hybrid Gold-Silicon Nano Particles in a Liquid. *Sci. Rep.* **2017**, *7*, 2045−2322.

(19) Taheri, M.; Hajiesmaeilbaigi, F.; Motamedi, A.; Golian, Y. Nonlinear Optical Response of Gold/Silicon Nanocomposite Prepared by Consecutive Laser Ablation. *Laser Phys.* **2015**, *25*, 065901.

(20) Zograf, G. P.; Zuev, D. A.; Milichko, V. A.; Mukhin, I. S.; Baranov, M. A.; Ubyivovk, E. V.; Makarov, S. V.; Belov, P. A. Laser Printing of Au/Si Core-Shell Nanoparticles. *J. Phys.: Conf. Ser.* **2016**, *741*, 012119.

(21) Makarov, S. V.; Sinev, I. S.; Milichko, V. A.; Komissarenko, F. E.; Zuev, D. A.; Ushakova, E. V.; Mukhin, I. S.; Yu, Y. F.; Kuznetsov, A. I.; Belov, P. A.; et al. Nanoscale Generation of White Light for Ultrabroadband Nanospectroscopy. *Nano Lett.* **2018**, *18*, 535−539.

(22) Saraeva, I. N.; Luong, N. V.; Kudryashov, S. I.; Rudenko, A. A.; Khmelnitskiy, R. A.; Shakhmin, A. L.; Kharin, A. Y.; Ionin, A. A.; Zayarny, D. A.; Tung, D. H.; et al. Laser Synthesis of Colloidal Si@Au and Si@Ag Nanoparticles in Water via Plasma-Assisted Reduction. *J. Photochem. Photobiol., A* **2018**, *360*, 125−131.

(23) Duff, D. G.; Baiker, A.; Edwards, P. P. A New Hydrosol of Gold Clusters. 1. Formation and Particle Size Variation. *Langmuir* **1993**, *9*, 2301−2309.

(24) Palik, E. *Handbook of Optical Constants of Solids*; Academic Press handbook series; Elsevier Science: 1998.

(25) Johnson, P. B.; Christy, R. W. Optical Constants of the Noble Metals. *Phys. Rev. B* **1972**, *6*, 4370−4379.

(26) Mun, J.; So, S.; Rho, J. Spectrally Sharp Plasmon Resonances in the Near Infrared: Subwavelength Core-shell Nanoparticles. *Phys. Rev. Appl.* **2019**, *12*, 044072.

(27) Nigoghossian, K.; Ouellet, S.; Plain, J.; Messaddeq, Y.; Boudreau, D.; Ribeiro, S. J. L. Upconversion Nanoparticle-Decorated Gold Nanoshells for Near-Infrared Induced Heating and Thermometry. *J. Mater. Chem. B* **2017**, *5*, 7109−7117.

(28) Saini, A.; Maurer, T.; Lorenzo, I. I.; Santos, A. R.; Béal, J.; Goffard, J.; Gérard, D.; Vial, A.; Plain, J. Synthesis and SERS Application of SiO2@Au Nanoparticles. *Plasmonics* **2015**, *10*, 791−796.

(29) Park, S. E.; Park, M. Y.; Han, P. K.; Lee, S. W. The Effect of pH-Adjusted Gold Colloids oh the Formation of Gold clusters over APTMS-Coated Silica Cores. *Bull. Korean Chem. Soc.* **2006**, *27*, 1341−1345.

(30) Park, S.; Park, M.; Han, P.; Lee, S. Relative Contributions of Experimental Parameters to NIR-Absorption Spectra of Gold Nanoshells. *J. Ind. Eng. Chem.* **2007**, *13*, 65−70.

(31) Wang, K.; Wang, Y.; Wang, C.; Jia, X.; Li, J.; Xiao, R.; Wang, S. Facile Synthesis of High-Performance SiO2@Au Core−Shell Nanoparticles with High SERS Activity. *RSC Adv.* **2018**, *8*, 30825−30831.

(32) Zyuzin, M. V.; Baranov, D. G.; Escudero, A.; Chakraborty, I.; Tsypkin, A.; Ushakova, E. V.; Kraus, F.; Parak, W. J.; Makarov, S. V. Photoluminescence Quenching of Dye Molecules Near a Resonant Silicon Nanoparticle. *Sci. Rep.* **2018**, *8*, 6107.

(33) Li, J.; Inukai, K.; Takahashi, Y.; Tsuruta, A.; Shin, W. Effect of PVP on the Synthesis of High-Dispersion Core−Shell Barium-Titanate−Polyvinylpyrrolidone Nanoparticles. *J. Asian Ceram. Soc.* **2017**, *5*, 216−225.

(34) Sugimoto, H.; Fujii, M. Colloidal Dispersion of Subquarter Micrometer Silicon Spheres for Low-Loss Antenna in Visible Regime. *Adv. Opt. Mater.* **2017**, *5*, 1700332.

(35) Ishii, S.; Sugavaneshwar, R. P.; Chen, K.; Dao, T. D.; Nagao, T. Solar Water Heating and Vaporization with Silicon Nanoparticles at Mie Resonances. *Opt. Mater. Express* **2016**, *6*, 640−648.

(36) Bardhan, R.; Grady, N. K.; Ali, T.; Halas, N. J. Metallic Nanoshells with Semiconductor Cores: Optical Characteristics Modified by Core Medium Properties. *ACS Nano* **2010**, *4*, 6169−6179.

(37) Höller, R. P. M.; Dulle, M.; Thomä, S.; Mayer, M.; Steiner, A. M.; Förster, S.; Fery, A.; Kuttner, C.; Chanana, M. Protein-Assisted Assembly of Modular 3D Plasmonic Raspberry-like Core/Satellite Nanoclusters: Correlation of Structure and Optical Properties. *ACS Nano* **2016**, *10*, 5740−5750.

(38) Wang, H.; Wen, J.; Wang, W.; Xu, N.; Liu, P.; Yan, J.; Chen, H.; Deng, S. Resonance Coupling in Heterostructures Composed of Silicon Nanosphere and Monolayer WS2: A Magnetic-Dipole-Mediated Energy Transfer Process. *ACS Nano* **2019**, *13*, 1739−1750.

(39) Proust, J.; Bedu, F.; Chenot, S.; Soumahoro, I.; Ozerov, I.; Gallas, B.; Abdeddaim, R.; Bonod, N. Chemical Alkaline Etching of Silicon Mie Particles. *Adv. Opt. Mater.* **2015**, *3*, 1280−1286.

(40) Manna, U.; Lee, J.-H.; Deng, T.-S.; Parker, J.; Shepherd, N.; Weizmann, Y.; Scherer, N. F. Selective Induction of Optical Magnetism. *Nano Lett.* **2017**, *17*, 7196−7206.

(41) Movsesyan, A.; Baudrion, A.-L.; Adam, P.-M. Revealing the Hidden Plasmonic Modes of a Gold Nanocylinder. *J. Phys. Chem. C* **2018**, *122*, 23651−23658.

(42) Gouesbet, G.; Grehan, G. Generalized Lorenz-Mie Theory for Assemblies of Sspheres and Aggregates. *J. Opt. A: Pure Appl. Opt.* **1999**, *1*, 706−712.

(43) Li, C.; Lee, S.; Qian, Z.; Woods, C.; Park, S.-J.; Fakhraai, Z. Controlling Magnetic Dipole Resonance in Raspberry-like Metamolecules. *J. Phys. Chem. C* **2018**, *122*, 6808−6817.

(44) Sheikholeslami, S. N.; Alaeian, H.; Koh, A. L.; Dionne, J. A. A Metafluid Exhibiting Strong Optical Magnetism. *Nano Lett.* **2013**, *13*, 4137−4141.

(45) Qian, Z.; Hastings, S. P.; Li, C.; Edward, B.; McGinn, C. K.; Engheta, N.; Fakhraai, Z.; Park, S.-J. Raspberry-like Metamolecules Exhibiting Strong Magnetic Resonances. *ACS Nano* **2015**, *9*, 1263−1270.

(46) Yang, H.; Li, B. Q.; Jiang, X.; Shao, J. Hybrid Nanostructure of SiO2@Si with Au-Nanoparticles for Surface Enhanced Raman Spectroscopy. *Nanoscale* **2019**, *11*, 13484−13493.

(47) Bohren, C. F.; Huffman, D. R. *Absorption and Scattering of Light by Small Particles*; John Wiley & Sons: Inc.: New York, 1983.